

pubs.acs.org/Macromolecules Article

Hybridization of a Bimodal Distribution of Copolymer Micelles

² Dan Zhao, En Wang, and Timothy P. Lodge*



Cite This: https://dx.doi.org/10.1021/acs.macromol.0c01419



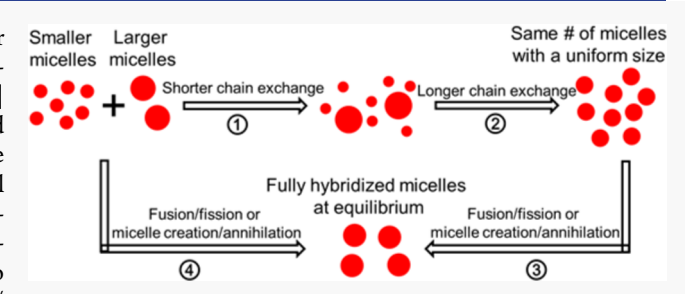
ACCESS

III Metrics & More

Article Recommendations

Supporting Information

3 **ABSTRACT:** The hybridization of two diblock copolymer 4 micelles in mixtures of ionic liquids, 1-ethyl and 1-butyl-3-5 methylimidazolium bis(trifluoromethylsulfonyl)imide ([EMIM] 6 and [BMIM][TFSI], or EMIM and BMIM in short), was studied 7 by time-resolved dynamic light scattering (DLS) and small-angle 8 X-ray and neutron scattering (SAXS/SANS). Two poly(methyl 9 methacrylate)-block-poly(n-butyl methacrylate) (PMMA-b-10 PnBMA) copolymers, where PnBMA and PMMA are the core-11 and corona-forming blocks, respectively, were employed. The two 12 diblocks have the same corona block molecular weight (25 000 g/



13 mol) but core block lengths differing by a factor of 2.2 (24 000 and 53 000 g/mol). Both polymers assemble into spherical micelles 14 in mixed ionic liquid solvents containing 0-30 wt % BMIM, albeit with different sizes. The solvent selectivity decreases with 15 increasing BMIM content. Time-resolved SANS quantified the unimer exchange time for each copolymer as a function of solvent 16 composition. In the most selective solvent (100% EMIM), the longer chains exchanged $\sim 10^4$ times more slowly than the shorter 17 ones; this difference was reduced to a factor of ca. 50 in 30% BMIM. The two micelle solutions in a given solvent were then mixed in 18 equal proportions, and the structural evolution of the blended micelles was monitored over several months. From previous work, we 19 know that at equilibrium the two copolymers should form a uniform population of mixed ("hybridized") micelles, with size 20 intermediate between the precursor micelles (albeit closer to the larger ones). In the more selective solvents, both light and neutron 21 scattering show that the apparent weight-average molecular weight (M_w) of the micelles initially increases with time, while SAXS 22 shows an increase in the average micelle core size. These observations reflect a net transfer of shorter chains from smaller to larger 23 micelles, as the shorter-chain exchange is much more facile but, in a certain sense, takes the system further away from equilibrium. 24 The long-time evolution monitored by DLS shows that the process of micellar hybridization depends greatly on solvent selectivity. 25 In 100% EMIM, Mw continues increasing even after several months, indicating that equilibrium is not reached within the 26 experimental time scale. For less selective solvents, the micelle size eventually begins to decrease and approaches the equilibrium 27 size, indicating that a unimer exchange of both molecular weights is operative. In the least selective solvent, 30% BMIM and both M., 28 and the average hydrodynamic size of the micelles start to decrease immediately and ultimately approach the values of the 29 equilibrium micelles. However, this process must involve other relaxation mechanisms, e.g., micelle fusion/fragmentation or micelle 30 creation/annihilation, as the total number of micelles also needs to be adjusted. Overall, this work exposes the possibility of different 31 routes to equilibrium for a given system and thereby underscores the complexity of equilibration in block copolymer micelles.

12 INTRODUCTION

33 Self-assembly of block copolymers into various micellar anostructures in a selective solvent has great potential to 55 enable a host of diverse applications. To facilitate these 36 applications, a fundamental understanding of the thermody-37 namic and dynamic characteristics of block copolymer micelles 38 is important. Over the past few decades, the equilibrium 39 structure of polymeric micelles has been well studied by both 40 theory and experiment. Over the past few decades, the equilibrate tion mechanisms have also been extensively investigated. It is generally accepted that micelle equilibration relies on 44 some combination of three processes: molecular exchange, 45 micelle creation/annihilation, and micelle fusion/fragmentation. When the system is close to equilibrium, molecular exchange is dominant, while when the system is far away from

the thermodynamically stable state, the other two processes are 48 more effective. In the past decade, progress has been made in 49 understanding the unimer exchange process near equilibrium, 50 especially by time-resolved small-angle neutron scattering (TR- 51 SANS). It has been found that the kinetics of chain exchange 52 depends on many molecular characteristics, including core 53 block length and dispersity, 20,27 corona block length, 28,29 54 solvent selectivity, micellar size and morphology, 32,33 and 55 micelle concentration. 34 However, in practice, the formulation 56

Received: June 17, 2020 Revised: August 13, 2020



57 of block copolymer micelles often leads to a nonequilibrated 58 state, which might gradually relax toward equilibrium. The 59 equilibration process is generally complicated, involving 60 multiple mechanisms, which remains to be clearly resolved.

Several studies have been designed to understand the 62 nonequilibrium relaxation processes of block copolymer 63 micelles. In some cases, sudden thermodynamic changes 64 (e.g., temperature or solvent selectivity) were introduced into 65 an equilibrated system and the following structural evolution in 66 the micelles was examined. 35-39 In others, various micelle 67 preparation protocols (e.g., direct dissolution or cosolvent 68 removal) yield kinetically trapped micellar morphologies, 69 which were then annealed and monitored. For instance, for 70 polybutadiene-block-poly(ethylene oxide) (PB-b-PEO) in 71 imidazolium-based ionic liquids, the initially formed poly-72 disperse and large micellar aggregates relax into smaller and 73 narrowly distributed spherical micelles upon annealing at high 74 temperatures, predominantly via fragmentation. 21,22,40,41 Addi-75 tionally, Kelley et al. have reported that, upon removal of 76 cosolvent, PB-b-PEO micelles in water slowly grow through a 77 distinct bimodal distribution separated by multiple fusion 78 events. 42 Note that in both these systems, no unimer exchange 79 was observed. 42,43

A third class of experiment follows the relaxation of mixtures 81 of micelles, i.e., micelle hybridization, which is the primary 82 focus of this report. A first hybridization experiment was 83 performed by Cantu and co-workers, 44 who measured the light 84 scattering intensity upon mixing two different micelles and 85 found that the equilibration time could be related to the critical 86 micelle concentration (CMC) of the individual micelles. 87 Furthermore, it was concluded that the formation time of 88 mixed micelles correlates with the unimer exchange rates. 89 Subsequently, Tian et al. studied micelle hybridization by 90 sedimentation velocity and found that the rate of hybridization 91 depends on the copolymer architecture and the thermody-92 namic properties of the solvent mixture. 45 In particular, it was 93 reported that hybridization did not occur if the solvent is very 94 poor for the core-forming block. More recently, Cai and 95 coauthors studied the hybridization of coil-rod-like copolymer 96 micelles by a combination of static and dynamic light 97 scattering and found that, upon mixing, larger hybrid micelles 98 were formed at the expense of each kind of the "pure" 99 micelles. 46 It was argued that the driving force for hybrid-100 ization comes from the entropy gain and the space-filling as the 101 core block is rodlike. Despite these interesting studies, there 102 are still many open questions about micelle hybridization that 103 have not been fully addressed: (i) what are the relative roles of 104 chain exchange or other processes (e.g., fusion/fragmentation 105 and formation of new micelles/disintegration of existing 106 micelles) in micelle hybridization? (ii) what are the possible 107 hybridization pathways? and (iii) how does the solvent 108 selectivity affect the micelle hybridization?

To provide some insight into these questions, we study the hybridization of two different micelles formed by poly(methyl methacrylate)-block-poly(n-butyl methacrylate) (PMMA-b-112 PnBMA, "MB") diblock copolymers in mixtures of the ionic liquids (ILs) 1-ethyl-3-methylimidazolium and 1-butyl-3-114 methylimidazolium bis(trifluoromethylsulfonyl)imide, 115 [EMIM][TFSI] and [BMIM][TFSI], respectively. Previous work has shown that PMMA is soluble in both ILs and forms the micelle corona, while PnBMA is insoluble in both solvents (with a lower critical solution temperature, LCST) and is thus 119 segregated in the micellar core. 47 Note that BMIM is a less

selective solvent than EMIM. The two diblocks have the same 120 corona chain length (N_{corona}), while the core block length 121 $(N_{\rm core})$ differs by a factor of 2.2. We have previously 122 established that for this pair of copolymers the equilibrium 123 state is a uniform population of mixed (hybrid) micelles at any 124 mixing ratio.⁴⁸ We first prepare pure micelles of each individual 125 copolymer and then blend them together to examine the time 126 evolution of micelle hybridization by a combination of 127 dynamic light scattering (DLS) and small-angle X-ray and 128 neutron scattering (SAXS/SANS). We also investigate the role 129 of solvent selectivity (by varying the composition of the IL 130 mixture) on micelle hybridization. Based on these results, we 131 discuss the role of chain exchange and other processes on 132 micelle hybridization and propose possible hybridization 133 pathways. All of the experiments were conducted at 55 °C 134 unless otherwise noted, which is much higher than the glass- 135 transition temperature $(T_{\rm g})$ of PnBMA $(T_{\rm g} \approx 20~{\rm ^{\circ}C})$; ⁴⁹ thus, 136 frozen dynamics due to glassy cores is not an issue. ^{50,51}

■ EXPERIMENTAL SECTION

Synthesis and Characterization. Hydrogenated and partially 139 deuterated (h- and d-) versions of the two diblock copolymers, 140 PMMA-b-PnBMA, were synthesized by sequential radical addition— 141 fragmentation chain-transfer (RAFT) polymerization. The partially 142 deuterated n-butyl methacrylate (d_9 -nBMA) monomer was prepared 143 by the reaction of methacryloyl chloride and d_{10} -n-butanol. The 144 synthetic details can be found in previous reports. The molecular 145 weights of the individual blocks and the dispersity of the diblocks 146 were thoroughly characterized by a combination of size exclusion 147 chromatography (SEC) with a multiangle light scattering detector 148 (MALS, Wyatt DAWN) and 1 H nuclear magnetic resonance 149 spectroscopy (1 H NMR, Varian Inova 500). The characterization 150 details were also described previously. Table 1 shows the physical 151 t1 characteristics of the diblocks.

138

Table 1. Characteristics of Diblock Copolymers^a

polymer	$\frac{M_{ m n,PMMA}}{(m kg/mol)}^b$	$M_{ m n,PnBMA}^{M$	$N_{ m PMMA}^{c}$	$N_{ m PnBMA}^{c}$	D^d
MB(25- 24)	25	24	250	169	1.05
MB(25- 25) <i>d</i>	25	25	250	166	1.05
MB(25- 53)	25	53	250	373	1.08
MB(25- 54)d	25	54	250	354	1.09

"As reported previously." 30 $^{b}M_{\rm n,PMMA}$ and $M_{\rm n,PnBMA}$ are the number-averaged molecular weights of the PMMA and PnBMA blocks, respectively. $^{c}N_{\rm PMMA}$ and $N_{\rm PnBMA}$ are the degrees of polymerization of the two blocks. ^{d}D is the dispersity of the diblock copolymer measured by SEC-MALS.

Ion-exchange reactions were performed to prepare the ionic liquids. 153 Specifically, [EMIM][TFSI] was obtained from the reaction of 154 [EMIM]Br and Li[TFSI], while [BMIM][TFSI] was synthesized by 155 the reaction of [BMIM]Cl and Li[TFSI]. To realize the contrast- 156 matching condition in the neutron scattering experiments, partially 157 deuterated versions of the two ILs were also prepared via isotopic 158 exchange of the three hydrogens on the imidazole ring with 159 deuterated water at 100 °C for 72 h. 53 The degree of deuteration 160 was quantified by ¹H NMR spectroscopy. All other chemicals were 161 purchased from Sigma-Aldrich and used as received.

Sample Preparation. The cosolvent method was used to prepare 163 the individual micellar solutions (larger micelles from MB(25-53) 164 and smaller ones from MB(25-24)) with a copolymer concentration 165 of 0.5 or 1 wt %. Briefly, the dried copolymer and an appropriate 166

Table 2. Characterization of Individual Micelles in Different Solvents

solvent	micelle	$R_{\rm h}$ (nm)	μ_2/Γ^{2a}	$R_{\rm c}$ (nm)	$\sigma_{ m R}$ (nm)	$L_{ m corona} \ (m nm)^b$	$N_{ m agg}^{c}$
0% BMIM	MB(25-24)	23.2	0.06	10.2	1.1	13.0	108
	MB(25-25)d	23.2	0.04	10.0	1.3	13.2	103
	MB(25-53)	29.3	0.03	16.9	1.5	12.4	221
	MB(25-54)d	28.0	0.04	16.7	1.6	11.3	225
10% BMIM	MB(25-24)	n.d. ^d	n.d. ^d	n.d. ^{<i>d</i>}	n.d. ^{<i>d</i>}	n.d. ^{<i>d</i>}	n.d. ^d
	MB(25-53)	28.7	0.03	16.8	1.6	11.9	217
20% BMIM	MB(25-24)	24.5	0.11	9.7	1.2	14.8	92
	MB(25-53)	29.2	0.04	16.7	1.6	12.5	213
30% BMIM	MB(25-24)	24.8	0.12	9.3	1.3	15.5	81
	MB(25-53)	28.4	0.03	15.7	1.4	12.7	177

^aAveraged over five scattering angles. $^bL_{\rm corona}$ is the corona thickness, estimated as $R_{\rm h}-R_{\rm c}$. $^cN_{\rm agg}$ is calculated as $4\pi R_{\rm c}^{~3} \varphi/(3\nu_{\rm PnBMA})$, where the polymer volume fraction in the core is $\varphi\approx0.9$, which was measured in a previous report in 0% BMIM. The $N_{\rm agg}$ values in other solvents should be viewed with caution as φ could be smaller than 0.9. $\nu_{\rm PnBMA}$ is the volume per core block. Not determined.

167 amount of IL were dissolved in good solvent dichloromethane 168 (DCM). Following that, DCM was slowly evaporated via a nitrogen purge until constant solution weight was achieved. The obtained 170 micellar dispersions were further dried at 50 °C for 12 h under vacuum (<100 mTorr). Complete removal of the cosolvent was confirmed by ¹H NMR spectroscopy. The individually prepared larger 173 and smaller micellar solutions were thoroughly mixed in either equal weight (SAXS, DLS) or equal core block volume (SANS) proportions 175 for subsequent time-resolved scattering experiments, as described 176 below. The mixed micellar solutions made by this protocol are referred to as "postmixed". In contrast, samples with the same overall compositions were also prepared by the "premixed" protocol, i.e., by first molecularly mixing the two diblocks with ILs together in DCM 180 and then slowly removing DCM to form hybridized micelles. The two 181 different protocols were adopted here to examine the thermodynamic 182 state of the postmixed samples upon long-time thermal annealing; the 183 premixed micelles are assumed to be close to the equilibrium state.

Dynamic Light Scattering (DLS). DLS experiments were performed on a Brookhaven BI-200SM instrument, with a laser 186 wavelength of 637 nm. Prior to the measurement, the micelle solution 187 was filtered with a 0.45 μ m poly(tetrafluoroethylene) (PTFE) filter 188 into a glass tube. It was then degassed under vacuum and flame-sealed 189 or sealed with parafilm. All light scattering experiments were 190 performed at 55 °C after at least 10 min of thermal equilibration. 191 To obtain the hydrodynamic radius (R_h) of the micelles, the 192 normalized intensity autocorrelation function, $g^{(2)}(t)$, was acquired at 193 five different angles (from 50 to 130°) for 10 min at each angle. The 194 second-order cumulant method was used to describe $g^{(2)}(t)$, from which the average decay rate $(\overline{\Gamma})$ and hydrodynamic size dispersity 196 $(\mu_2/\overline{\Gamma}^2)$ of the micelles can be obtained. ⁵⁴ Note that the definition of 197 size dispersity for micelles is different from that for polymer chains. 198 We use different definitions in current work, as they are convention-199 ally used and accepted in the polymer community. Following that, a 200 linear fit of $\overline{\Gamma}$ vs q^2 gives the average diffusion coefficient (D_m) . Here 201 $q = (4\pi n/\lambda) \sin(\theta/2)$ is the scattering vector, where n is the IL 202 refractive index, λ is the laser wavelength in vacuum, and θ is the scattering angle. From D_m, R_h can be calculated from the Stokes-Einstein relation, i.e., $R_h = k_B T/(6\pi\eta D_m)$, where k_B is the Boltzmann 205 constant, T is the absolute temperature, and η is the solvent viscosity. 206 On the other hand, for the time-resolved light scattering experiments, 207 the two micelle solutions (0.5 wt % copolymer) were combined in a 208 1:1 weight ratio and well mixed by magnetic stirring at room 209 temperature. The resulting mixed solution was then quickly filtered 210 into the glass tube, which was degassed and flame-sealed as described 211 above. The delay time, i.e., that between solution mixing and the first 212 measurement, was about 30 min, including the 10 min thermal 213 equilibration at 55 °C. The measurement was performed at an angle 214 of 90° for 10 min at each time point, during which the scattering 215 intensity I(t) and hydrodynamic radius R_h were monitored. Note that 216 there is typically a notable random fluctuation in I(t), attributable to 217 the ionic liquid solvents. However, the average I(t) is quite

reproducible (with a 1% deviation). Additionally, the scattering 218 intensity of an ionic liquid sample was also measured at each time 219 point. This was then used to normalize the scattering intensity of the 220 micellar mixture solutions to account for any potential change in the 221 laser intensity over time. Between the long-time measurements, the 222 solution was isothermally annealed in an oil bath at 55 °C. Due to the 223 nonvolatility of ionic liquids, the change in polymer concentration 224 during long thermal annealing can be neglected (also the glass tube 225 was flame-sealed).

Small-Angle X-ray Scattering (SAXS). The SAXS experiments 227 were performed on the 5-ID-D beamline (Dupont-Northwestern- 228 Dow Collaborative Access Team) at the Argonne National 229 Laboratory (Advanced Photon Source). The accessible scattering 230 vector q range was $\sim 0.0025 - 0.19 \text{ Å}^{-1}$, using a wavelength λ of 0.73 Å 231 and a sample-to-detector distance of 8.50 m. For these measurements, 232 1 wt % micelle solutions were transferred into 1.5 mm diameter quartz 233 capillary tubes (Charles Supper Company). The capillary tubes were 234 then sealed with epoxy. The measurement temperature was 55 °C. 235 Isotropic two-dimensional (2D) scattering data were acquired by a 236 Rayonix CCD area detector for 0.5 or 1 s, which was then converted 237 into the one-dimensional (1D) traces, i.e., scattering intensity I(q) vs 238 q. The scattering data were then background-corrected using the 239 corresponding solvent in the capillary tube and analyzed by the 240 Pedersen model for block copolymer micelles with the Percus-Yevick 241 hard-sphere structure factor.

Small-Angle Neutron Scattering (SANS). The SANS experi- 243 ments were performed on the GP-SANS CG-2 instrument at the High 244 Flux Isotope Reactor (HFIR) facility at Oak Ridge National 245 Laboratory (ORNL). The neutron wavelength of the neutron beam 246 was 4.75 Å (with a spread of $\Delta \lambda/\lambda = 0.13$) and the sample-to-detector 247 distance was 10 m, which provided a q range of $\sim 0.007-0.1 \text{ Å}^{-1}$. To 248 measure the chain exchange kinetics of individual micelles, as 249 described previously, 30,33 two populations of micelles (protonated 250 and deuterated, 1 wt %) were prepared in a contrast-matching solvent 251 mixture, the scattering length density of which equals the average of 252 the protonated and deuterated core blocks. Note that the PMMA 253 corona chains in both micelles are protonated. Afterward, different 254 amounts of the two micelle solutions (corresponding to equal core 255 block volumes) were thoroughly mixed at specified temperatures (25, 256 35, and 55 °C), quickly transferred into 1 mm banjo cells, and placed 257 on the beamline for data acquisition. Due to the redistribution of the 258 h- and d- chains among different populations of micelles, the 259 scattering intensity I(q, t) will decrease with time and ultimately 260 approach that of the fully hybridized, premixed sample, $I(q, \infty)$. Here 261 the premixed sample was prepared by blending the same amounts of 262 h- and d-chains in a good solvent (DCM), which was then removed 263 by nitrogen purge. Thus, micelles prepared by this route should have 264 an equal volume of h- and d-core blocks on average in each micelle. 265

To quantify the rate of chain exchange, we adopt the normalized 266 relaxation function, defined as 19 267

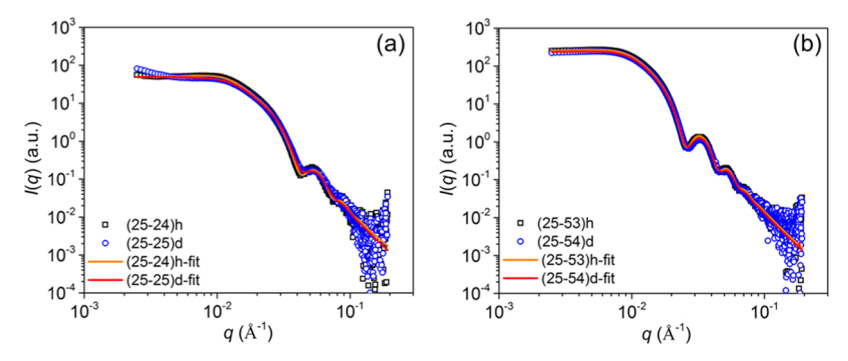


Figure 1. SAXS intensity I(q) vs scattering vector q for 1 wt % micelle solutions in [EMIM][TFSI]. Panel (a) represents MB(25–24) and MB(25–25)d and panel (b) represents MB(25–53) and MB(25–54)d. The symbols represent the experimental data and the lines correspond to best fits to the Pedersen model.

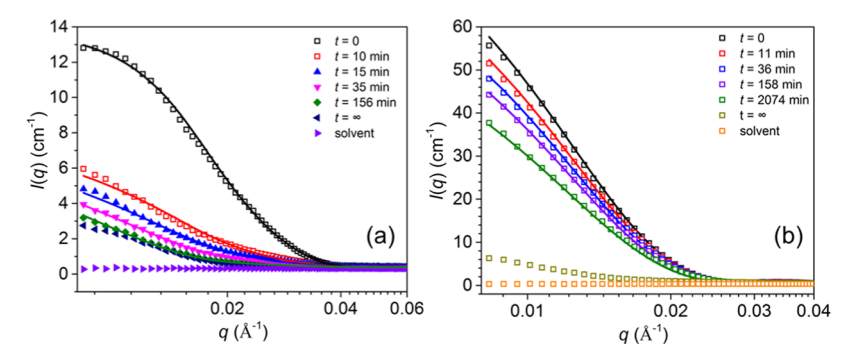


Figure 2. Representative TR-SANS profiles I(q) vs q for 1 wt % postmixed micellar solutions of (a) MB(25–24) and MB(25–25)d and (b) MB(25–53) and MB(25–54)d in contrast-matching [EMIM][TFSI] at 55 °C and varying times. Note that " $t = \infty$ " represents the premixed sample. The symbols represent the experimental data and the lines correspond to the calculation, as detailed in the text.

$$R(t) = \sqrt{\frac{I(q, t) - I(q, \infty)}{I(q, 0) - I(q, \infty)}}$$

$$\tag{1}$$

Here, I(q, 0) is the scattering intensity at time t = 0, which was 270 estimated by the average scattering intensity of the corresponding h-271 and d-micelles, as chain exchange occurs at room conditions. 272 Similarly, the chain exchange of the hybrid micelles was measured 273 by mixing equal core block volumes of protonated larger and 274 deuterated smaller micelles. Additionally, the scattering intensity of 275 mixtures of protonated larger and smaller micelles in the deuterated 276 solvent was also measured as a function of time. In all of these time-277 resolved runs, the 2D scattering data were recorded in 5 min intervals 278 for 2–3 h, which was then reduced and converted into 1D profiles 279 using a custom-made program at ORNL.

80 RESULTS

268

f1

281 We first characterize the structure of individual protonated/ 282 deuterated (h-/d-) larger and smaller micelles via a 283 combination of DLS, SAXS, and SANS, with the results 284 presented in Table 2. Unless otherwise noted, the data were 285 acquired with the hydrogenated version of the micelles and all 286 of the measurements were performed at 55 °C. Note that it has 287 been previously shown that the structure of these micelles 288 barely changes with temperature under these experimental 289 conditions. 33,52 DLS shows a single, narrowly distributed 290 population of micelles formed by either the shorter, MB(25– 291 24), or the longer, MB(25-53), diblocks (Figure S1). The 292 average hydrodynamic radius and size dispersity in EMIM are 293 23.2 nm and 0.06 for the smaller and 29.3 nm and 0.03 for the 294 larger micelles, respectively. Figure 1 shows the SAXS profiles 295 of 1 wt % protonated/deuterated micelles in EMIM. Analysis 296 based on the Pedersen model with a hard-sphere structure

factor yields structural parameters including the average 297 micelle core size (R_c) and dispersity; R_c was 10.2 and 16.9 298 nm for the smaller and larger micelles, respectively, with 299 standard deviations of 1.1 and 1.5 nm. Very similar values were 300 obtained for the corresponding deuterated versions (Table 2). 301 The micelle structure was also characterized by SANS, which 302 provides similar core sizes and dispersity between the 303 protonated and deuterated micelles for each copolymer. 304 However, as shown in Figure S2, the scattering profiles 305 between the h- and d-micelles are visually distinct, due to the 306 different scattering length densities of the h- and d-cores of the 307 micelles (more details are provided in the Supporting 308 Information). On the basis of these results, other structural 309 parameters can be estimated. For instance, the difference 310 between $R_{\rm h}$ and $R_{\rm c}$ was taken as the average corona thickness. 311 The mean aggregation number can also be estimated under the 312 reasonable assumption that there is $\sim 10\%$ solvent (or $\sim 90\%$ $_{313}$ polymer) in the micelle core. ⁴⁸ All of the structural $_{314}$ characteristics of the individual micelles in different solvents 315 are shown in Table 2.

We next examine the chain exchange kinetics of the two 317 individual micelles. Figure 2 shows the evolution of the 318 f2 scattering intensity with time at 55 °C for both micelles in 319 EMIM. In each case, the scattering intensity monotonically 320 drops with time, reflecting the redistribution of h- and d-chains 321 via the unimer exchange process. Clearly, the chain exchange 322 rate of the smaller micelles is much greater than the larger 323 ones, as evidenced by the larger decrease in intensity after a 324 given time. Integration of the scattering intensity (over the q 325 range of $0.008-0.04 \, \text{Å}^{-1}$ for MB(25-24) and $0.008-0.03 \, \text{Å}^{-1}$ 326 for MB(25-53)) and following eq 1, the relaxation function 327

R(t) can be calculated and is presented in Figure S3. To 329 facilitate comparison, the R(t) curves at different temperatures 330 were then time-temperature-superposed at a reference 331 temperature of 35 °C (Figure 4a). The superposed R(t) can 332 be well described by the model proposed by Choi et al., 20 in 333 which two fitting parameters were obtained: $\alpha \chi$ and the 334 dispersity of the core block (N_w/N_p) , where α is a scale factor 335 and χ is the Flory–Huggins parameter between the core block 336 and the solvent. For the smaller micelles MB(25-24), $\alpha \gamma =$ 337 0.030 and $N_w/N_p = 1.10$, while for larger micelles MB(25-53), 338 $\alpha \chi = 0.035$ and $N_{\rm w}/N_{\rm n} = 1.15$. Following the model of Choi et 339 al., the characteristic relaxation time for chain exchange is given 340 by $\tau \sim N_{\text{core}}^2 \exp(\alpha \chi N_{\text{core}})$. Thus, the unimer exchange for the 341 smaller micelles is about 4 orders of magnitude faster than that 342 of the larger ones, primarily due to the difference in the core 343 block length. This is consistent with earlier reports that the 344 molecular exchange in diblock copolymer micelles is hypersensitive to the core block length. 20,27,30

Next, the hydrogenated larger and deuterated smaller micelles were mixed, with the scattering intensity of the micellar mixture monitored as a function of time (Figure 3).

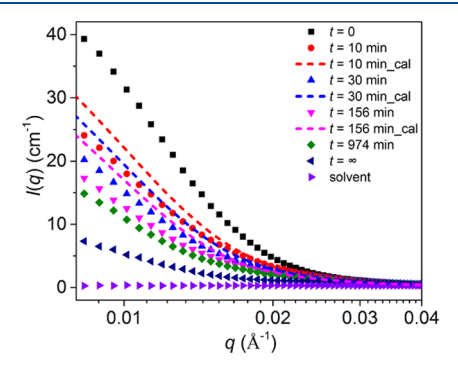


Figure 3. Representative TR-SANS profiles I(q) vs q for 1 wt % postmixed micellar solutions of MB(25–53) and MB(25–25)d in contrast-matching [EMIM][TFSI] at 55 °C and varying times. Note that $t = \infty$ represents the premixed sample. The symbols represent the experimental data and the dashed lines correspond to the calculation, as described in the text.

349 Again, the scattering intensity progressively decreases with 350 time. This clearly indicates that there is "crosstalk", or 351 exchange, between the two populations of micelles; if there 352 were only chain exchange among the same population of 353 micelles, the scattering intensity would remain constant.

Similar treatment of the data as that for individual micelles $_{354}$ yields R(t) for the micellar mixture. Figure 4a shows that R(t) $_{355}$ f4 decreases continuously with time and falls in between that of $_{356}$ the larger and smaller micelles, which is intuitively reasonable. $_{357}$ Similar results were obtained in another solvent, i.e., $_{20\%}$ $_{358}$ BMIM (Figure S4). We have to note that, for calculation of $_{359}$ R(t) for the micellar mixture, $I(q, \infty)$ is assumed to be that of $_{360}$ the premixed micelles, which could be a good first $_{361}$ approximation but might not be exact, as discussed later in $_{362}$ the text. Thus, some caution needs to be taken in interpreting $_{363}$ the R(t) data of the micellar mixture. Additionally, the SANS $_{364}$ experiments were performed up to $_{16}$ h, which only accesses $_{365}$ the relatively short-time hybridization. The long-time process $_{366}$ will be examined by time-resolved light scattering complemented by SAXS.

Figure 5 shows the time dependence of the average 369 f5 hydrodynamic radius R_h (Figure 5a) and the normalized 370 scattering intensity (Figure 5b) of 0.5 wt % postmixed micellar 371 mixtures of MB(25-24) and MB(25-53) in varying solvents 372 at 55 °C. Note that the experimental time here is up to 53- 373 223 days, depending on the solvent. As shown in Figure 5, in 374 EMIM (i.e., 0% BMIM), both $R_{\rm h}$ and the scattering intensity 375 increase with annealing time. Consistent results were found 376 from SANS (Figure S5). At 10% BMIM, the average micelle 377 size and scattering intensity first increase with time and then 378 apparently level off. At both 15 and 20% BMIM, the intensity 379 shows a clear maximum with time; $R_{\rm h}$ vs t is also consistent 380 with this behavior, albeit with greater scatter. By 30% BMIM, 381 there is barely any change in either R_h and I(t) during the early 382 stage of hybridization, and then both decrease at longer times, 383 ultimately approaching the values of the premixed sample. 384 Concurrently, the size dispersity of the micellar mixtures was 385 also monitored during these time-resolved experiments, as 386 shown in Figure S6. There is no systematic change in size 387 dispersity with time, presumably due to the fact that the R_b of 388 the two micelles are not that different (<25%) and there is a 389 significant overlap in the size distributions (Figure S1). 390 Overall, the micellar mixture can reach the thermodynamically 391 stable state only in the least selective solvent (i.e., 30% 392 BMIM), as indicated by the fact that in this case similar 393 micellar structures were obtained via preparation from two 394 different routes (postmixed vs premixed). In contrast, in the 395 other solvents, even after annealing for several months, the $R_{\rm h}$ 396 and I(t) of the postmixed micellar mixtures are still 397 substantially larger than that obtained from the premixing 398

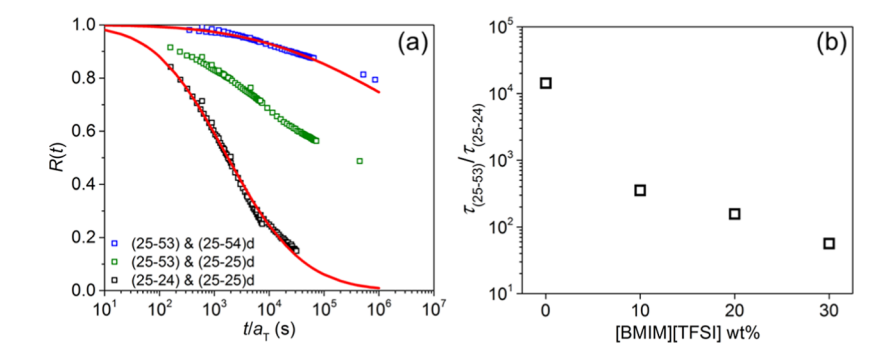


Figure 4. (a) Time–temperature-superposed R(t) vs t/a_T for 1 wt % postmixed micellar solutions in contrast-matching [EMIM][TFSI]. The reference temperature is 35 °C. The symbols represent the experimental data and the red lines correspond to the best fits to the model proposed by Choi et al.²⁰ (b) Ratio of the chain exchange time of MB(25–53) and MB(25–24) ($\tau_{MB(25-53)}/\tau_{MB(25-24)}$) vs the weight fraction of [BMIM][TFSI] in the solvent mixture.

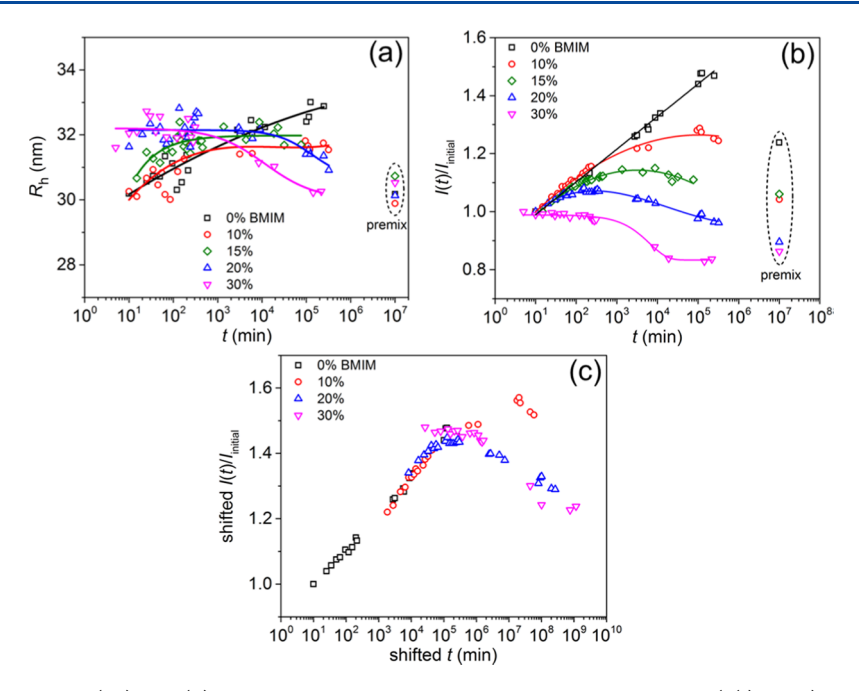


Figure 5. (a) Hydrodynamic radius (R_h) and (b) normalized background-corrected scattering intensity ($I(t)/I_{initial}$) vs the mixing time t for 0.5 wt % postmixed micellar solutions of MB(25–24) and MB(25–53) in varying solvents at a scattering angle of 90° and a temperature of 55 °C. Note that the data points at " $t = 10^7$ min" correspond to the premixed samples with identical content. The symbols are the experimental data and the solid lines are drawn as guides to the eye. (c) Shifted normalized scattering intensity ($I(t)/I_{\text{initial}}$) based on data in (b)) vs the shifted mixing time t. Note that the time shift factors are based on the different chain exchange times of the larger micelles in varying solvents. Additionally, the normalized intensities were arbitrarily vertically shifted to construct the master curve. The vertical shift factors are 1, 1.22, 1.34, and 1.48, respectively, for 0, 10, 20, and 30% [BMIM][TFSI]. Finally, the reference for all of the data shifts is the "0% BMIM".

399 protocol (Figure 5b). In Figure 5c, we present a "master curve" 400 for the mixed micelle equilibration process, by shifting the 401 intensity versus time curves both vertically and horizontally. 402 This is an empirical and nonrigorous procedure, but it reveals 403 important aspects of the process. In particular, an early-time growth in the average micelle size and scattered intensity is 405 apparent, followed by a long-time decay toward the 406 equilibrium state. The early-time increase is interesting, in 407 that it appears to represent a trajectory in phase space that 408 begins by moving further away from equilibrium, prior to 409 reversing course. The horizontal shift is based on the unimer 410 exchange time of the longer chains and correlates with 411 variation in solvent selectivity; the less selective the solvent, the 412 more rapid the equilibration, and a certain selectivity is 413 necessary to access the regime of the early-time increase. The 414 selectivity is manifest in the separation of the time scales for unimer exchange for shorter and longer chains (Figure 4b), as 416 will be discussed further below.

Figure 6a—e presents the SAXS traces in the five solvents, the respectively. Each panel includes data for the premixed sample, the postmixed sample at t=0, and a postmixed sample after long-time annealing at 55 °C (from 53 to 223 days). Note that the annealed postmixed solutions correspond to the last data points in Figure 5a,b; the premixed and postmixed solutions last appearance in Figure 5a,d,e, upon annealing for a long time, the shown in Figure 6a,d,e, upon annealing for a long time, the last I(q) traces of the postmixed solutions display significant last changes in the intermediate I(q) traces and dispersity form factor scattering). Specifically, minima (or slight depressions) in the scattering curves in this I(q) range shift to lower I(q) indicating an apparent increase in the average micelle last core size of the micellar mixtures. This observation is

consistent with the in situ SANS data (Figure S7). Addition- 432 ally, a distinct dip in each curve appears in each solvent after 433 annealing. Comparing the scattering data of the premixed (red $_{434}$ symbols) and postmixed solutions after long-time annealing 435 (black symbols), significant differences still persist in the 436 intermediate q range in all solvents except 30% BMIM. 437 Interestingly, the intensity gap between the two solutions 438 seems to be progressively smaller as the solvent becomes less 439 selective toward the core block (i.e., the fraction of BMIM 440 increases). In particular, in 30% BMIM, the two scattering 441 curves nearly overlap, indicating almost the same micellar 442 structure between premixed and postmixed samples, suggestive 443 of full equilibration. This is consistent with the results from 444 light scattering (Figure 5). To quantify structural disparities 445 between the premixed and annealed postmixed solutions, the 446 scattering data were fit to the Pedersen model (for postmixed 447 solutions, a sum of two polydisperse block copolymer micelles 448 was adopted), and the fits are also shown in Figure 6 (green 449 lines). The obtained R_c and σ_R values for each fit are 450 summarized in Table S1. A few salient points are noted here. 451 First, the core size of the premixed solutions lies between the 452 larger and smaller populations of the postmixed solutions after 453 annealing. Second, in 0, 10, and 15% BMIM, the larger 454 micelles in the postmixed samples are even larger than in the 455 pure individual larger micelles. For instance, in 0% BMIM, R_c 456 of MB(25-53) and the larger population in the postmixed 457 micellar mixture are 16.9 and 18.8 nm, respectively. On the 458 other hand, in 20 and 30% BMIM, the two sizes are very 459 similar (16.7 vs 16.6 nm in 20% BMIM and 15.7 vs 15.4 nm in 460 30% BMIM). Additionally, the sizes of the pure individual 461 smaller micelles and the smaller population in the postmixed 462 micellar mixture are comparable (e.g., 10.2 vs 10.3 nm and 9.3 463

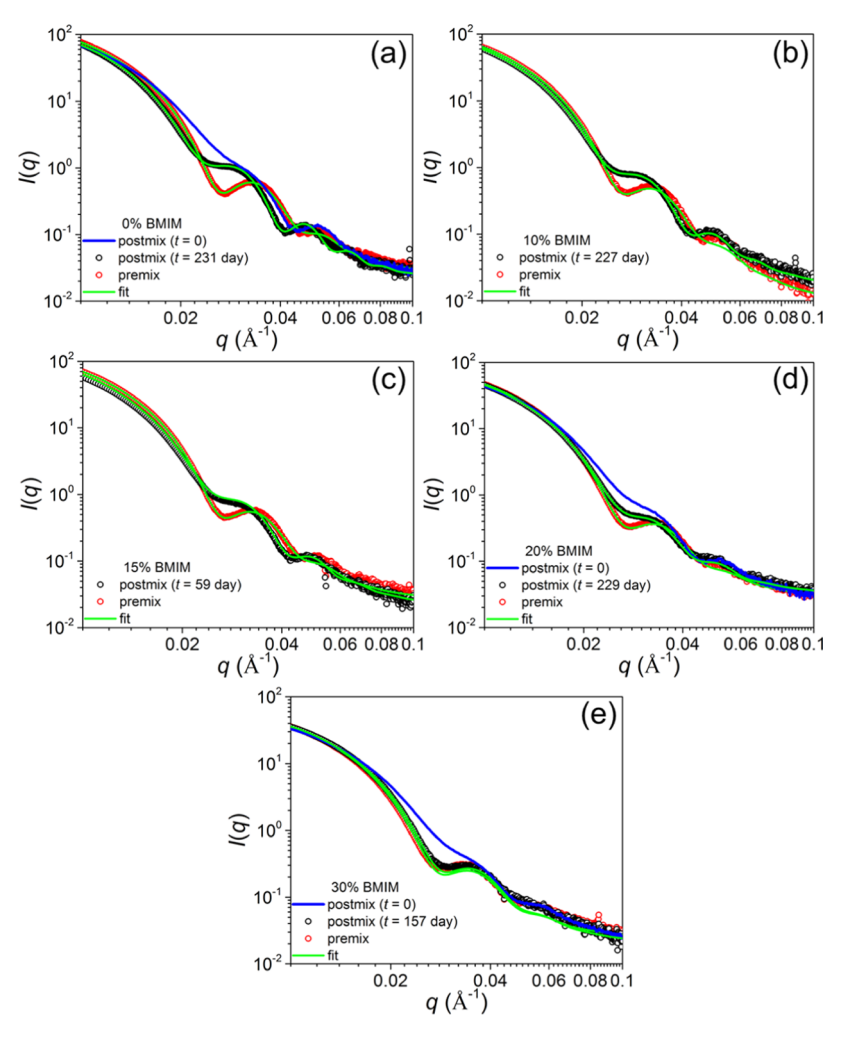


Figure 6. SAXS intensity I(q) vs q for 0.5 wt % premixed and postmixed micellar solutions in (a) EMIM (0 wt % BMIM), (b) 10 wt % BMIM, (c) 15 wt % BMIM, (d) 20 wt % BMIM, and (e) 30 wt % BMIM at 55 °C. The black symbols represent the premixed samples and the red symbols correspond to postmixed solutions upon annealing at 55 °C for varying amounts of time. The green curves represent the best fits to the Pedersen model. Note that the premixed and postmixed solutions in each graph have identical total compositions but different sample histories. The blue lines are the scattering intensities of postmixed solutions at t = 0, which were calculated as the average of I(q) of the individual micelles. For clarity, the data are shown only for the q range of 0.01-0.1 Å⁻¹; the complete data are provided in the Supporting Information.

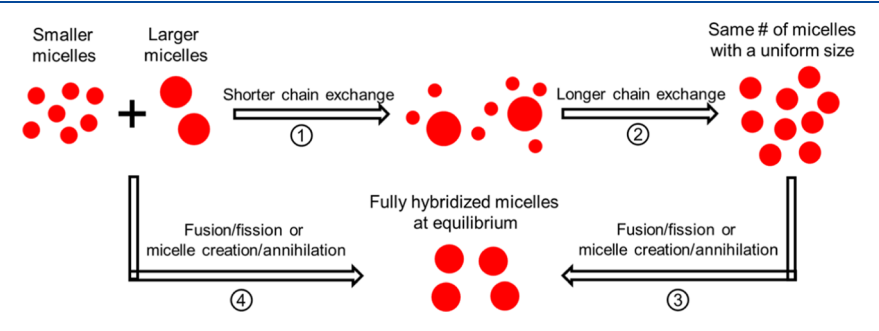


Figure 7. Schematic description of the micelle hybridization processes in different pathways. For simplicity, the red spheres represent micelles of varying sizes, roughly to the scale. The number of circles roughly corresponds to the number ratios of the smaller and larger micelles in current work. The four processes are briefly described as (1) dominated by the shorter-chain exchange, (2) the longer-chain exchange becomes facile, (3) and (4) structural reorganization via fusion/fission and micelle creation/annihilation mechanisms.

464 vs 9.8 nm in 0 and 30% BMIM, respectively). These results are 465 fully consistent with the results in Figure 5.

466 DISCUSSION

Here the Before discussing the mechanisms of micelle hybridization, we Here the thermodynamically stable state of

the mixed micellar system. A good first approximation should $_{469}$ be that resulting from the premixed protocol. In this scenario, $_{470}$ our previous report has revealed that these two diblocks are $_{471}$ able to co-micellize and form a single, relatively narrowly $_{472}$ distributed population of mixed micelles, at all mixing ratios. $_{473}^{48}$ This is because the disparity of the core block length between $_{474}$

475 the two diblocks is not that large; as a result, well-mixed 476 micelles are thermodynamically more favorable than a binary 477 micellar mixture of different sizes. Figure 7 presents a general 478 overview of possible mechanisms for hybridizing micellar 479 mixtures. There are three processes involved: chain exchange, 480 fusion/fragmentation, and formation of new micelles from 481 unimers/disintegration of existing micelles. In the case of chain 482 exchange, the shorter-chain exchange will be dominant at the 483 very beginning, as the rate of exchange is very sensitive to the 484 core block chain length. This process will make the smaller 485 micelles become even smaller and larger ones become even 486 larger (step 1 in Figure 7) and could explain the increase in 487 scattering intensity in Figure 5b,c. At longer times, the longer-488 chain exchange becomes facile, and the transfer of longer 489 chains to smaller micelles will make the micelle sizes more 490 uniform, ultimately leading to hybridized micelles with uniform 491 size (step 2 in Figure 6). Note, however, that the chain 492 exchange itself cannot adjust the number of micelles in the 493 system. Therefore, to fully equilibrate the system, at least one 494 of the other two processes (fusion/fission or micelle creation/ 495 annihilation) needs to be involved (step 3 in Figure 7). This 496 two-stage micelle relaxation mechanism, i.e., first relaxation by 497 unimer exchange and then equilibration of the total number of 498 micelles, has been proposed in the theoretical study of 499 Nyrkova and Semenov, 58 which agrees well with the 500 interpretation in current work. As noted above, previous work has shown that the equilibrium state is a uniform population of spherical micelles, each containing a mixture of 503 long and short chains, with an intermediate size. However, 504 because of the relief of chain stretching in a "mixed" core, the 505 size of the hybrid micelle is much closer to that of the larger 506 precursor. 48 The scattering intensity decrease in Figure 5c 507 could reflect either step 2 or step 3 or a combination of both. It 508 should be emphasized that, although steps 1-3 are drawn as 509 occurring in series, they are independent and likely occur at the 510 same time, i.e., in parallel, especially steps 2 and 3. As discussed 511 further below, this will depend on the solvent selectivity. On 512 the other hand, even if there is no chain exchange, in principle, 513 equilibration to a fully hybridized state could still occur via the 514 other two mechanisms (step 4 in Figure 7).^{21,22}

The short-time structural reorganization is presumably 516 dominated by chain exchange mechanism in the current system, particularly that of the shorter chains (step 1). The 518 chain exchange rate of the shorter diblocks is much greater 519 (e.g., by ~4 orders of magnitude in 0% BMIM), so there is a 520 net flux of shorter chains to larger micelles. This accounts for 521 the short-term increase in the size of the larger micelles 522 (Figures 5a, 6, and S7, except in 30% BMIM) and, accordingly, 523 a decrease in the smaller micelle size. As a result, the weight-524 averaged molecular weight (M_w) of the micelles in the mixture 525 increases, leading to an increase in the scattering intensity 526 (Figures 5b and S5; $I \sim KcM_{wt}$ where K is the optical constant 527 and c is the copolymer concentration). Notably, this process is 528 reminiscent of Ostwald ripening in colloid systems. The 529 transfer of some shorter chains to larger micelles could be 530 thermodynamically favorable, as the interfacial energy per chain is lower in the larger micelles.

To quantify the role of chain exchange in the early stages of system hybridization, we performed the following calculation based on the TR-SANS data. First, for both individual larger and smaller micelles, we estimated the "survival" fraction f(t) of h- and d-system remaining in the original h- and d-micelles after chain exchange time t, either from R(t) or by fitting to the scattering

data of postmixed h- and d-micelles at time t (the solid lines in 538 Figure 2). The relationship between f(t) and R(t) (derived in 539 the Supporting Information, and note R(t) here refers to an 540 individual micelle) is

$$f(t) = \frac{R(t) + 1}{2} \tag{2}_{542}$$

Therefore, the fraction of chains that has been expelled and 543 redistributed $f(t)_{\text{expelled}}$ is 544

$$f(t)_{\text{expelled}} = 2(1 - f(t))$$
 (3) 545

This can be extended to the mixture of larger and smaller 546 micelles, assuming independent chain exchange⁵⁹ in hybridized 547 micelles (i.e., micelles containing both longer and shorter 548 chains) and that the expelled chains are reinserted into the 549 larger and smaller micelles with equal probability. Also, we 550 assume that the number of larger and smaller micelles are both 551 constant. On this basis, the average micelle core size and core 552 scattering length density of each population can be calculated 553 at any time. For instance, at time t of mixing, the fraction of 554 chains expelled from each larger and smaller micelle is 555 $f(t)_{\rm expelled,L}$ and $f(t)_{\rm expelled,S}$. The net transfer of shorter core 556 blocks to larger micelles is $(f(t)_{\rm expelled,S} n_{\rm L})/(n_{\rm L} + n_{\rm S})$, where $n_{\rm L}$ 557 and $n_{\rm S}$ are the number densities of the larger and smaller 558 micelles, respectively. Similarly, the net transfer of longer core 559 blocks to smaller micelles is $(f(t)_{\text{expelled,L}} n_{\text{S}})/(n_{\text{L}} + n_{\text{S}})$. Take 560 the larger micelle population, the volume fraction of core 561 blocks in solution at time t is

$$\nu_{L,t} = \nu_{L,0} \left(1 - \frac{f(t)_{\text{expelled,L}} n_{\text{S}}}{n_{\text{L}} + n_{\text{S}}} + \frac{f(t)_{\text{expelled,S}} n_{\text{L}}}{n_{\text{L}} + n_{\text{S}}} \right)$$
(4) 56:

where $\nu_{\rm L,0}$ is the volume fraction of longer core blocks in 564 solution at zero time. The core size of the larger micelles will 565 be updated as

$$R_{\mathrm{L},t} = \left(R_{\mathrm{L},0}^{3} \frac{\nu_{\mathrm{L},t}}{\nu_{\mathrm{L},0}}\right)^{1/3} \tag{5}$$

where $R_{L,0}$ is the larger micelle core size at time 0. The volume 568 fraction of shorter core blocks in the larger micelle core is 569

$$\nu_{s,L,t} = \left(\frac{f(t)_{\text{expelled,S}} n_{\text{L}}}{n_{\text{L}} + n_{\text{S}}}\right) / \left(1 - \frac{f(t)_{\text{expelled,L}} n_{\text{S}}}{n_{\text{L}} + n_{\text{S}}}\right) + \frac{f(t)_{\text{expelled,S}} n_{\text{L}}}{n_{\text{L}} + n_{\text{S}}}\right) \times (1 - \varphi_{s,c})$$
(6) 570

where $\varphi_{s,c}$ is the volume fraction of the solvent in the micellar s71 core. Similarly, the volume fraction of longer core blocks in the s72 larger micelle core $\nu_{l,l,t}$ can be calculated. Hence, the average s73 scattering length density in the core of the larger micelles is

$$\rho_{\text{core,L},t} = \rho_{\text{core,d}} \nu_{\text{s,L},t} + \rho_{\text{core,h}} \nu_{\text{l,L},t} + \rho_{\text{s}} \varphi_{\text{s,c}}$$

$$(7)_{\text{s75}}$$

where $\rho_{\text{core},h'}$ $\rho_{\text{core},h'}$ and ρ_{s} are the scattering length densities of 576 the d-, h- core blocks, and the solvent, respectively. Similarly, 577 the volume fraction, core size, and scattering length density of 578 the smaller micelles can be calculated. With these parameters 579 being updated, the scattering intensity of the micellar mixture 580 after mixing time t can be calculated (the dashed lines in 581 Figure 3). As can be seen, the measured intensities are 582 systematically lower than the calculated ones for all three 583 mixing times. A few factors could lead to this deviation. First, 584

585 expelled chains could be preferentially reinserted into one 586 population over the other. For instance, the expelled shorter 587 chains might favorably go to the larger micelles to reduce the 588 interfacial energy; on the other hand, the expelled longer 589 chains could enter the smaller micelles with a much higher 590 probability, as they can help reduce the shorter core block 591 stretching. 48 Alternatively, new micelles could form from a 592 direct hybridization of free unimers in solution. 46 Both 593 scenarios would accelerate the redistribution of the h- and d-594 chains among the larger and smaller micelles, thus leading to a 595 more rapid drop in scattering intensity, as observed in Figure 596 3; the former explanation seems more probable, given the failure to fully equilibrate most of the mixtures at long times. Although the scattering intensity increases at short times 599 upon mixing of micelles in all solvents (except 30% BMIM; 600 Figure 5b), the rate of increase goes up with solvent selectivity. 601 One likely cause is that $au_{\mathrm{MB}(25-53)}/ au_{\mathrm{MB}(25-24)}$ decreases with the weight fraction of BMIM in the solvent mixture, as shown in Figure 4b. Presumably, the larger mismatch in the unimer exchange of the two populations of micelles in highly selective 605 solvents (e.g., 0% BMIM) effectively transfers more shorter 606 chains to larger micelles, thus resulting in a more rapid increase 607 in the scattering intensity. On the other hand, in 30% BMIM, 608 the scattering intensity barely changes with time in the early 609 stage of hybridization, which could be accounted for by several 610 reasons. First, it is likely that the initial structural change upon 611 mixing of micelles in this solvent is too fast to capture by the 612 light scattering experiment due to the delay in sample preparation (~30 min). Alternatively, as discussed above, the 614 time scale for chain exchange differs only by a factor of ~50 615 (Figure 4b), and for the two micelles of equal total core block 616 volume, the number of smaller micelles is ~4 times that of the 617 larger ones. This makes the net transport of chains between the 618 two populations of micelles more balanced, thus leading to less 619 change in the scattering intensity. Additionally, other processes 620 (formation of new micelles or fusion/fragmentation) could 621 also be invoked at an earlier time scale in this solvent. For 622 instance, there should be more free chains due to lower solvent 623 selectivity, which will facilitate the assembly of new micelles 624 from the direct hybridization of different unimers.

Next, we discuss the hybridization mechanisms at long 626 times, focusing on the distinct feature that the scattering intensity in Figure 5b starts to decrease with time (except in 628 0% BMIM). The time scale where the intensity starts to drop 629 correlates with increasing solvent selectivity. To examine how 630 this is related to unimer exchange, the time axis in Figure 5 was 631 shifted by the ratio of the chain exchange time relative to that 632 in 0% BMIM, which was taken as the reference. Two different 633 ways of time shifting were performed, based on the differences 634 in the chain exchange time of either smaller (Figure S8) or 635 larger micelles (Figure 5c). Apparently, that calculated from 636 the larger micelles can better superpose the intensity vs time 637 curves in various solvents (Figure 5c). This reflects the fact 638 that the scattered intensity is dominated by the larger micelles 639 and that the chain exchange of the larger micelles is the rate-640 limiting step (Figure 7). However, other processes such as 641 fusion/fragmentation or micelle annihilation/creation must be 642 involved to fully equilibrate the micellar mixture, and they 643 could also contribute to the intensity decrease in Figure 5b,c. 644 Assuming that the premixed samples are good approximants of 645 the equilibrium states, only the micellar mixture in the 30% 646 BMIM is able to reach the equilibrium within the experimental 647 time scale of 7 months. This indicates that, even in micellar

systems where chain exchange is facile, it is still difficult or even 648 impossible to fully equilibrate within a reasonable time frame. 649 For micellar mixtures in 0–20% BMIM, the structure of the 650 postmixed micelles after long-time annealing is still signifi-651 cantly different from the premixed counterparts (Figures 5 and 652 6). Detailed analyses of the SAXS data (Figure 6) reveal that 653 there are still two distinct populations of micelles even after 654 long-time annealing, with the size of the larger population 655 being greater than the pure individual larger micelles. In fact, to 656 reach the equilibrium state, the number of micelles in the 657 postmixed solution needs to be adjusted, again suggesting that 658 the other two relaxation processes must be involved, as chain 659 exchange itself cannot adjust the number of micelles (Figure 660 7). Table 3 summarizes the structure and number of micelles 661 t3

Table 3. Characterization of Individual, Premixed, and Postmixed Micelles

		$R_{\rm c}$		# of micelles (total block copolymer
solvent	micelle	(nm)	$N_{ m agg}^{a}$	weight of 10^{-15} g) ^b
0% BMIM	MB(25- 24)	10.2	108	114
	MB(25- 53)	16.9	221	35
	postmix	c	с	$114 + 35 = 149^d$
	premix	16.3	301	66 ^e
20% BMIM	MB(25- 24)	9.7	92	133
	MB(25- 53)	16.7	213	36
	postmix	c	С	$133 + 36 = 169^d$
	premix	16.2	293	68 ^e
30% BMIM	MB(25- 24)	9.3	81	151
	MB(25- 53)	15.7	177	44
	postmix	c	с	$151 + 44 = 195^d$
	premix	15.1	238	84 ^e

 $^aN_{\rm agg}$ the aggregation number of micelles, was estimated as described in Table 2, assuming that the polymer volume fraction in the core is $\sim\!0.9$ in all cases. b The number of micelles for a total mass of 10^{-15} g for either shorter and longer diblocks. The number of micelles for the premix and postmix solutions corresponds to a total mass of 2×10^{-15} g. c Not applicable. d The total number of micelles (sum of smaller and larger ones) upon mixing or at zero mixing time. c The number of premixed micelles with equal masses $(10^{-15}$ g) of shorter and longer diblocks.

for both premixed and postmixed hybrids. In all three solvents, 662 the number of micelles in the premixed solution is much 663 smaller than the sum of smaller and larger micelles in the 664 postmixed solution. For example, in 30% BMIM, as shown in 665 Table 3, the number of micelles in the premixed solution (on 666 the basis of a total mass of each diblock of 10^{-15} g) is 84, while 667 the sum of the number of smaller and larger micelles in the 668 postmixed solution at zero time is 195. This indicates that the 669 number of micelles needs to be reduced by more than half in 670 the hybridization process. Presumably, most of the smaller 671 micelles disintegrate by being incorporated into the existing 672 larger micelles or forming new micelles. Similar calculations 673 were performed in the other two solvents, 0 and 20% BMIM, 674 with similar results.

Finally, we summarize the hybridization processes in 676 solvents of varying selectivity. In a highly selective solvent 677 (e.g., 0% BMIM), the unimer exchange between the two 678 populations of micelles results in a dominant transport of 679

I

680 shorter chains to larger micelles, making the larger micelles 681 become even larger and smaller ones even smaller. This 682 process seems to continue even after annealing for more than 7 683 months, leading to a kinetically trapped state that cannot be 684 fully relaxed within the experimental time scale. On the other 685 hand, in a weakly selective solvent (e.g., 30% BMIM), the 686 postmixed and premixed micellar mixtures are able to reach the 687 same thermodynamic state, indicating that equilibrium is 688 obtained. We propose the following pathways. At short times, 689 chain exchange is the dominant mechanism (steps 1 and 2 in 690 Figure 7), but eventually, micelle fusion/fragmentation or 691 micelle creation/annihilation occurs. Unimer exchange makes 692 the micelle size disparity even larger, which actually brings the 693 system farther away from equilibrium. This might favor the 694 process of fragmentation, which is more probable when the 695 micelles are too large. Additionally, "unidirectional" 696 chain exchange could make the smaller micelles less stable, such that they break apart into unimers. Also, the nucleation 698 and growth of new micelles definitely require a continuous 699 supply of free chains from existing micelles, which could be 700 realized via the chain expulsion process. Therefore, although 701 the other two mechanisms are required to fully hybridize the 702 two micelles (steps 3 and 4 in Figure 7), chain exchange/ 703 expulsion still plays a critical role in the entire hybridization 704 process.

705 SUMMARY

706 In this report, we have investigated the hybridization of two 707 different sized micelles in ionic liquids of varying selectivity. 708 We first characterized the structure and chain exchange 709 kinetics of the two pure individual micelles. It was found 710 that both the shorter and longer diblocks self-assemble into 711 well-defined spherical micelles with different sizes. Addition-712 ally, due to the difference in the core block length, the rate of 713 chain exchange is much higher in smaller micelles than in 714 larger ones. The two micellar solutions were mixed, and the 715 hybridization process was monitored by time-resolved SANS 716 and light scattering, complemented by SAXS. TR-SANS data 717 undoubtedly show that there is crosstalk between the two 718 populations of micelles. Specifically, in a highly selective 719 solvent, 0% BMIM, the scattering intensity continues to 720 increase even after annealing for more than 7 months, which 721 apparently results from the predominant transfer of shorter 722 chains to larger micelles, due to the several orders of 723 magnitude disparity in chain exchange rates of the two 724 micelles. This leads to a locally stable, kinetically trapped state 725 that cannot be equilibrated within the experimental time scale. 726 SAXS data confirm this conclusion and show the existence of 727 two distinct populations of micelles in the postmixed micellar 728 mixture even after long-time annealing. On the other hand, in a 729 much less selective solvent, 30% BMIM, two stages of micelle 730 hybridization were proposed. First, at short times, chain exchange should be the dominant process. This actually brings 732 the system farther away from equilibrium and thus invokes the other two relaxation mechanisms, micelle fusion/fragmentation or micelle creation/annihilation. All of these processes 735 combined together are able to fully hybridize the two micelles. 736 Therefore, both light and X-ray scattering show a similar 737 structure between the premixed and postmixed micellar 738 mixtures after long-time annealing. Our results suggest that 739 the micelle hybridization process depends greatly on the 740 solvent selectivity and the findings provide new insight into 741 how a micellar system transforms from a nonequilibrated to a

thermodynamically more stable state. TR-SANS can provide 742 detailed measurements of unimer exchange, but more 743 experimental studies of the kinetics of fusion, fragmentation, 744 and micelle annihilation/creation would be very useful.

ASSOCIATED CONTENT

Supporting Information

The Supporting Information is available free of charge at 748 https://pubs.acs.org/doi/10.1021/acs.macromol.0c01419. 749

DLS data, SANS data and analysis, additional time- 750 resolved SANS and DLS data, fitting results of SAXS 751 data on both premixed and postmixed solutions upon 752 long-time annealing, derivation of the relationship 753 between R(t) and f(t), and time-shifted light scattering 754 data (Figures S1–S9 and Table S1) (PDF) 755

746

747

756

757

762

769

770

772

773

AUTHOR INFORMATION

Corresponding Author

Timothy P. Lodge — Department of Chemistry and Department 758 of Chemical Engineering and Materials Science, University of 769 Minnesota, Minneapolis, Minnesota 55455, United States; 760 orcid.org/0000-0001-5916-8834; Email: lodge@umn.edu 761

Authors

Dan Zhao – Department of Chemistry, University of Minnesota, 763 Minneapolis, Minnesota 55455, United States; Oocid.org/ 764 0000-0001-8928-0691

En Wang — Department of Chemical Engineering and Materials 766 Science, University of Minnesota, Minneapolis, Minnesota 767 55455, United States; Oorcid.org/0000-0002-3271-7562 768

Complete contact information is available at: https://pubs.acs.org/10.1021/acs.macromol.0c01419

Notes 771

The authors declare no competing financial interest.

ACKNOWLEDGMENTS

We acknowledge financial support from the National Science 774 Foundation (DMR-1707578). Portions of this work were 775 performed at the DuPont-Northwestern-Dow Collaborative 776 Access Team (DND-CAT) located at Sector 5 of the 777 Advanced Photon Source (APS). DND-CAT is supported by 778 Northwestern University, E.I. DuPont de Nemours & Co., and 779 The Dow Chemical Company. This research used resources of 780 the Advanced Photon Source, a U.S. Department of Energy 781 (DOE) Office of Science User Facility operated for the DOE 782 Office of Science by the Argonne National Laboratory under 783 Contract No. DE-AC02-06CH11357. Additionally, a portion 784 of this research used resources at the High Flux Isotope 785 Reactor, a DOE Office of Science User Facility operated by the 786 Oak Ridge National Laboratory. We would like to thank Dr. 787 Lilin He for the assistance in SANS measurements and data 788 reduction and Dr. Yuanchi Ma for preparing the polymers.

REFERENCES

(1) He, Y.; Li, Z.; Simone, P.; Lodge, T. P. Self-assembly of block 791 copolymer micelles in an ionic liquid. *J. Am. Chem. Soc.* **2006**, 128, 792 2745–2750.

(2) Zhulina, E. B.; Adam, M.; LaRue, I.; Sheiko, S. S.; Rubinstein, M. 794 Diblock copolymer micelles in a dilute solution. *Macromolecules* **2005**, 795 38, 5330–5351.

- 797 (3) Kataoka, K.; Harada, A.; Nagasaki, Y. Block copolymer micelles 798 for drug delivery: design, characterization and biological significance. 799 *Adv. Drug Delivery Rev.* **2001**, *47*, 113–131.
- 800 (4) Attia, A. B. E.; Ong, Z. Y.; Hedrick, J. L.; Lee, P. P.; Ee, P. L. R.; 801 Hammond, P. T.; Yang, Y.-Y. Mixed micelles self-assembled from 802 block copolymers for drug delivery. *Curr. Opin. Colloid Interface Sci.* 803 **2011**, *16*, 182–194.
- 804 (5) Park, T. G.; Jeong, J. H.; Kim, S. W. Current status of polymeric 805 gene delivery systems. *Adv. Drug Delivery Rev.* **2006**, *58*, 467–486.
- 806 (6) Raffa, P.; Broekhuis, A. A.; Picchioni, F. Polymeric surfactants 807 for enhanced oil recovery: a review. *J. Pet. Sci. Eng.* **2016**, *145*, 723–808 733.
- 809 (7) Glass, R.; Möller, M.; Spatz, J. P. Block copolymer micelle 810 nanolithography. *Nanotechnology* **2003**, *14*, 1153–1160.
- 811 (8) Noolandi, J.; Hong, K. M. Theory of block copolymer micelles in 812 solution. *Macromolecules* **1983**, *16*, 1443–1448.
- 813 (9) Halperin, A. Polymeric micelles: a star model. *Macromolecules* 814 **1987**, 20, 2943–2946.
- 815 (10) Halperin, A.; Tirrell, M.; Lodge, T. P. Tethered chains in 816 polymer microstructures. *Adv. Polym. Sci.* **1992**, 27, 31–71.
- 817 (11) Riess, G. Micellization of block copolymers. *Prog. Polym. Sci.* 818 **2003**, 28, 1107–1170.
- 819 (12) Gohy, J.-F. Block copolymer micelles. *Adv. Polym. Sci.* **2005**, 820 190, 65–136.
- 821 (13) Mai, Y.; Eisenberg, A. Self-assembly of block copolymers. *Chem.* 822 Soc. Rev. **2012**, 41, 5969–5985.
- 823 (14) Atanase, L. I.; Riess, G. Self-assembly of block and graft 824 copolymers in organic solvents: An overview of recent advances. 825 *Polymers* **2018**, *10*, No. 62.
- 826 (15) Honda, C.; Hasegawa, Y.; Hirunuma, R.; Nose, T. Micellization 827 kinetics of block copolymers in selective solvent. *Macromolecules* 828 **1994**, 27, 7660–7668.
- 829 (16) Amann, M.; Diget, J. S.; Lyngsø, J.; Pedersen, J. S.; Narayanan, 830 T.; Lund, R. Kinetic pathways for polyelectrolyte coacervate micelle 831 formation revealed by time-resolved synchrotron SAXS. *Macro-832 molecules* **2019**, *52*, 8227–8237.
- 833 (17) Parent, L. R.; Bakalis, E.; Ramírez-Hernández, A.; Kammeyer, J. 834 K.; Park, C.; De Pablo, J.; Zerbetto, F.; Patterson, J. P.; Gianneschi, N. 835 C. Directly observing micelle fusion and growth in solution by liquid-836 cell transmission electron microscopy. *J. Am. Chem. Soc.* **2017**, *139*, 837 17140–17151.
- 838 (18) Dormidontova, E. E. Micellization kinetics in block copolymer 839 solutions: Scaling model. *Macromolecules* **1999**, 32, 7630–7644.
- 840 (19) Lund, R.; Willner, L.; Stellbrink, J.; Lindner, P.; Richter, D. 841 Logarithmic Chain-Exchange Kinetics of Diblock Copolymer 842 Micelles. *Phys. Rev. Lett.* **2006**, *96*, No. 068302.
- 843 (20) Choi, S.; Lodge, T. P.; Bates, F. S. Mechanism of Molecular 844 Exchange in Diblock Copolymer Micelles: Hypersensitivity to Core 845 Chain Length. *Phys. Rev. Lett.* **2010**, *104*, No. 047802.
- 846 (21) Early, J. T.; Lodge, T. P. Fragmentation of 1, 2-Polybutadiene-847 block-Poly(ethylene oxide) Micelles in Imidazolium-Based Ionic 848 Liquids. *Macromolecules* **2019**, *52*, 7089–7101.
- 849 (22) Early, J. T.; Yager, K. G.; Lodge, T. P. Direct Observation of 850 Micelle Fragmentation via in situ Liquid-Phase Transmission Electron 851 Microscopy. *ACS Macro Lett.* **2020**, *9*, 756–761.
- 852 (23) Rharbi, Y. Fusion and Fragmentation Dynamics at Equilibrium 853 in Triblock Copolymer Micelles. *Macromolecules* **2012**, *45*, 9823–854 9826.
- 855 (24) Rharbi, Y.; Li, M.; Winnik, M. A.; Hahn, K. G. Temperature 856 Dependence of Fusion and Fragmentation Kinetics of Triton X-100 857 Micelles. J. Am. Chem. Soc. 2000, 122, 6242–6251.
- 858 (25) Zana, R. Dynamics in Micellar Solutions of Amphiphilic Block 859 Copolymers. In *Dynamics of Surfactant Self-Assemblies: Micelles,* 860 Microemulsions, Vesicles, and Lyotropic Phases; Hubbard, A. T., Ed.;
- 861 Taylor & Francis Group/CRC Press: Boca Raton, 2005; pp 161–231.
 862 (26) Michels, B.; Waton, G.; Zana, R. Dynamics of Micelles of
- 863 Poly(Ethylene Oxide)-Poly (Propylene Oxide)-Poly(Ethylene Oxide)
- 864 Block Copolymers in Aqueous Solutions. *Langmuir* 1997, 13, 3111–865 3118.

- (27) Zinn, T.; Willner, L.; Lund, R.; Pipich, V.; Richter, D. 866 Equilibrium exchange kinetics in n-alkyl–PEO polymeric micelles: 867 single exponential relaxation and chain length dependence. *Soft Matter* 868 **2012**, *8*, 623–626.
- (28) Zinn, T.; Willner, L.; Pipich, V.; Richter, D.; Lund, R. 870 Molecular exchange kinetics of micelles: corona chain length 871 dependence. ACS Macro Lett. 2016, 5, 884–888.
- (29) Wang, E.; Lu, J.; Bates, F. S.; Lodge, T. P. Effect of corona 873 block length on the structure and chain exchange kinetics of block 874 copolymer micelles. *Macromolecules* **2018**, *51*, 3563–3571.
- (30) Ma, Y.; Lodge, T. P. Chain exchange kinetics in diblock 876 copolymer micelles in ionic liquids: The role of χ . *Macromolecules* 877 **2016**, 49, 9542–9552.
- (31) Wang, E.; Zhu, J.; Zhao, D.; Xie, S.; Bates, F. S.; Lodge, T. P. 879 Effect of solvent selectivity on chain exchange kinetics in block 880 copolymer micelles. *Macromolecules* **2020**, *53*, 417–426.
- (32) Lund, R.; Willner, L.; Pipich, V.; Grillo, I.; Lindner, P.; 882 Colmenero, J.; Richter, D. Equilibrium chain exchange kinetics of 883 diblock copolymer micelles: Effect of morphology. *Macromolecules* 884 **2011**, 44, 6145–6154.
- (33) Zhao, D.; Ma, Y.; Lodge, T. P. Exchange kinetics for a single 886 block copolymer in micelles of two different sizes. *Macromolecules* 887 **2018**, *51*, 2312–2320.
- (34) Choi, S. H.; Bates, F. S.; Lodge, T. P. Molecular exchange in 889 ordered diblock copolymer micelles. *Macromolecules* **2011**, *44*, 3594–890 3604.
- (35) Honda, C.; Abe, Y.; Nose, T. Relaxation Kinetics of 892 Micellization in Micelle-Forming Block Copolymer in Selective 893 Solvent. *Macromolecules* **1996**, *29*, 6778–6785.
- (36) Burke, S. E.; Eisenberg, A. Kinetics and mechanisms of the 895 sphere-to-rod and rod-to-sphere transitions in the ternary system 896 PS310-b-PAA52/dioxane/water. *Langmuir* **2001**, *17*, 6705–6714. 897
- (37) Landazuri, G.; Fernandez, V. A.; Soltero, J. F. A.; Rharbi, Y. 898 Kinetics of the sphere-to-rod like micelle transition in a pluronic 899 triblock copolymer. *J. Phys. Chem. B* **2012**, *116*, 11720–11727.
- (38) Denkova, A. G.; Mendes, E.; Coppens, M. O. Non-equilibrium 901 dynamics of block copolymer micelles in solution: recent insights and 902 open questions. *Soft Matter* **2010**, *6*, 2351–2357.
- (39) Halperin, A.; Alexander, S. Polymeric micelles: their relaxation 904 kinetics. *Macromolecules* **1989**, 22, 2403–2412.
- (40) Meli, L.; Lodge, T. P. Equilibrium vs metastability: High- 906 temperature annealing of spherical block copolymer micelles in an 907 ionic liquid. *Macromolecules* **2009**, *42*, 580–583.
- (41) Meli, L.; Santiago, J. M.; Lodge, T. P. Path-dependent 909 morphology and relaxation kinetics of highly amphiphilic diblock 910 copolymer micelles in ionic liquids. *Macromolecules* **2010**, 43, 2018—911 2027.
- (42) Kelley, E. G.; Murphy, R. P.; Seppala, J. E.; Smart, T. P.; Hann, 913 S. D.; Sullivan, M. O.; Epps, T. H. Size evolution of highly 914 amphiphilic macromolecular solution assemblies via a distinct 915 bimodal pathway. *Nat. Commun.* **2014**, *5*, No. 3599.
- (43) Won, Y. Y.; Davis, H. T.; Bates, F. S. Molecular exchange in 917 PEO-PB micelles in water. *Macromolecules* **2003**, *36*, 953–955.
- (44) Cantu, L.; Corti, M.; Salina, P. Direct measurement of the 919 formation time of mixed micelles. *J. Phys. Chem. A.* **1991**, 95, 5981–920 5983.
- (45) Tian, M.; Qin, A.; Ramireddy, C.; Webber, S. E.; Munk, P.; 922 Tuzar, Z.; Prochazka, K. Hybridization of block copolymer micelles. 923 *Langmuir* 1993, 9, 1741–1748.
- (46) Cai, P.; Wang, C.; Ye, J.; Xie, Z.; Wu, C. Hybridization of 925 polymeric micelles in a dispersion mixture. *Macromolecules* **2004**, *37*, 926 3438–3443.
- (47) Hoarfrost, M. L.; He, Y.; Lodge, T. P. Lower Critical Solution 928 Temperature Phase Behavior of Poly(*n*-butyl methacrylate) in Ionic 929 Liquid Mixtures. *Macromolecules* **2013**, *46*, 9464–9472.
- (48) Zhao, D.; Ma, Y.; Wang, E.; Lodge, T. P. Micellization of 931 Binary Diblock Co-polymer Mixtures in an Ionic Liquid. *Macro-932 molecules* **2019**, *52*, 4729–4738.

- 934 (49) Wiley, R. H.; Brauer, G. Refractometric determination of 935 second-order transition temperatures in polymers. II. Some acrylic, 936 vinyl halide, and styrene polymers. J. Polym. Sci. 1948, 3, 455–461. 937 (50) Wright, D. B.; Patterson, J. P.; Gianneschi, N. C.; Chassenieux, 938 C.; Colombani, O.; O'Reilly, R. K. Blending block copolymer micelles 939 in solution; obstacles of blending. Polym. Chem. 2016, 7, 1577–1583. 940 (51) Wang, Y.; Balaji, R.; Quirk, R. P.; Mattice, W. L. Detection of 941 the rate of exchange of chains between micelles formed by diblock 942 copolymers in aqueous solution. Polym. Bull. 1992, 28, 333–338. 943 (52) Ma, Y.; Lodge, T. P. Poly(methyl methacrylate)-block-poly(n-944 butyl methacrylate) diblock copolymer micelles in an ionic liquid: 945 Scaling of core and corona size with core block length. Macromolecules 946 2016, 49, 3639–3646.
- 947 (53) Dzyuba, S. V.; Li, S.; Bartsch, R. A. Convenient syntheses of 948 perdeuterated ionic liquids. *J. Heterocycl. Chem.* **2007**, *44*, 223–225. 949 (54) Frisken, B. J. Revisiting the method of cumulants for the 950 analysis of dynamic light-scattering data. *Appl. Opt.* **2001**, *40*, 4087–951 4091.
- 952 (55) Pedersen, J. S. Determination of size distribution from small-953 angle scattering data for systems with effective hard-sphere 954 interactions. *J. Appl. Crystallogr.* **1994**, 27, 595–608.
- 955 (56) Pedersen, J. S.; Gerstenberg, M. C. The structure of P85 956 Pluronic block copolymer micelles determined by small-angle neutron 957 scattering. *Colloids Surf., A* **2003**, *213*, 175–187.
- 958 (57) Pedersen, J. S.; Svaneborg, C.; Almdal, K.; Hamley, I. W.; 959 Young, R. N. A small-angle neutron and X-ray contrast variation 960 scattering study of the structure of block copolymer micelles: Corona 961 shape and excluded volume interactions. *Macromolecules* **2003**, *36*, 962 416–433.
- 963 (58) Nyrkova, I. A.; Semenov, A. N. On the theory of micellization 964 kinetics. *Macromol. Theory Simul.* **2005**, 14, 569–585.
- 965 (59) Lu, J.; Bates, F. S.; Lodge, T. P. Chain exchange in binary 966 copolymer micelles at equilibrium: Confirmation of the independent 967 chain hypothesis. *ACS Macro Lett.* **2013**, *2*, 451–455.